RSC Advances

PAPER

View Article Online
View Journal | View Issue

Cite this: *RSC Adv.*, 2023, **13**, 30499

Microfluidic paper-based colorimetric quantification of malondialdehyde using silver nanoprism toward *on-site* biomedical analysis: a new platform for the chemical sensing and biosensing of oxidative stress†

Farnaz Bahavarnia,[a] Hossein Navay Baghban,[b] Morteza Eskandani[a] and Mohammad Hasanzadeh *[c]

Malondialdehyde (MDA) is a critical product of polyunsaturated adipose acid peroxidation and represents a common biomarker of oxidative stress. The effect of different MDA concentrations on human biofluids reflects pathological changes, which has been seen in diverse types of sickness, such as leukemia, diabetes, cancer, cardiovascular disease, and age-related macular degeneration and liver disease. In this study, different types of silver nanoparticles, including silver nanoprism (AgNPrs), silver nanowires (AgNWs), and silver nanospheres (AgNSs), were synthesized and used for the chemosensing of MDA by colorimetric and spectrophotometric methods. Colorimetric tests were performed to identify malondialdehyde in the solution as well as the one-droplet-based microfluidic paper substrate as a miniaturization device for the monitoring of analytes in human real samples. The analytical quantification of the MDA was done using the UV-Vis method. Also, the utilization of the designed chemosensor for the analysis of MDA in real sample was evaluated in human urine samples. Using the spectrophotometric method, MDA was deformed in the linear range of 0.01192 to 1.192 mM with a low limit of quantification of 0.12 μM. Essential significant features of this study include the first application of AgNPrs with high stability and great optical properties without any reagent as an optical sensing probe of MDA and optimized OD-μPCD toward on-site and on-demand MDA screening in real samples diagnosis and the innovative time/color semi-analytical recognition strategy. Moreover, the prepared OD-μPCD decorated by AgNPrs could be a prized candidate for commercialization due to the benefits of the low-cost materials used, like paper and paraffin, and portability. This innovative process led to uniform hydrophilic micro-channels on the surface of cellulose, without the use of a UV lamp, clean room, and organic solvents. This report could be a pioneering work, inspiring simple and effective on-site semi-analytical recognition devices for harmful substances or illegal drugs, which simply consist of a piece of lightweight paper and one drop of the required reagent.

Received 11th September 2023
Accepted 2nd October 2023

DOI: 10.1039/d3ra06191d

rsc.li/rsc-advances

1. Introduction

Malondialdehyde (MDA) is an active and highly reactive aldehyde compound and is produced in the human body from the peroxidation of unsaturated fatty acids.[1] On the other hand, as MDA itself is an active and highly reactive compound by attacking other molecules, it affects the function of molecules and ultimately the function of the cell while forming a strong covalent bond.[2] MDA is a highly reactive compound that occurs in the enol form. MDA is easily deprotonated to give the sodium salt of the enolate. In neutral solution, MDA is present as the relatively unreactive enolate anion or at lower pH as the β-hydroxyacrolein and can thus form adduct by Michael addition and Schiff base formation. Under physiological conditions, MDA reacts primarily with the ε-amino groups of protein lysine residues and has been observed to cause protein cross-linking. MDA can form adducts with both proteins and DNA and has been shown to form DNA adducts even in the human liver devoid of any overt disease. MDA is one of the activated carbonyl cheek not only in various physiological pathways but in various pathologic processes as well, including Alzheimer's disease, diabetes, and cardiovascular diseases.[3] Also, the binding to

[a]*Research Center for Pharmaceutical Nanotechnology, Tabriz University of Medical Sciences, Tabriz, Iran*
[b]*Nutrition Research Center, Tabriz University of Medical Sciences, Tabriz, Iran*
[c]*Pharmaceutical Analysis Research Center, Tabriz University of Medical Sciences, Tabriz, Iran. E-mail: hasanzadehm@tbzmed.ac.ir*

† Electronic supplementary information (ESI) available. See DOI: https://doi.org/10.1039/d3ra06191d

purine bases in the DNA structure causes mutagenic, atherogenic, and carcinogenic properties.[4] So, by the monitoring of MDA in different biological samples, it is possible to understand the amount of peroxidation of fats and use it as an indicator to measure the level of oxidative stress in a living organism. Therefore, the development of the extension of a procedure for the detection of MDA in living systems is valuable for the diagnosis and treatment of related diseases.[5]

Various methods have been used to detect and determine MDA in different biofluids including fluorescence,[6] surface-enhanced Raman spectroscopy,[7] mass spectrometry,[8] capillary electrophoresis,[9] and the thiobarbituric acid (TBA) way.[10] However, some of these procedures are improper for on-the-spot detection because they require expensive tools and expertise.

The healthcare field is considered one of the most important pillars of any society, and it can be said that the development of this field is one of the criteria for the progress of a community.[11] This field can include many fields such as food and water health, diagnosis of diseases, and their treatment.[12] Today, many attempts have been made in order to improve food safety, but discussions such as food safety due to the wide scope, long process from production to consumption, and unavailability of advanced tests are still challenging issues in all societies.[13]

In the diagnosis of diseases, despite the use of modern methods and well-equipped tests, there are still disadvantages such as high costs, time-consuming nature of tests, need for skill in conducting tests and disease diagnosis, and the unavailability of routine tests for some areas.[14] For these reasons, there is a need to find cheap, portable kits without the need for external sources, which are available and easy to use in the field of diagnosing diseases using on-demand biomarkers analysis. Microfluidic devices have attracted the attention of many researchers in recent years.[15] Using this technology, it is possible to build integrated diagnostic systems with the ability of rapid analysis of biomarkers.[16]

Microfluidic systems for diagnostic usage have many advantages such as reducing the consumption of reagents shortening the reaction time, proper efficiency in performing the reaction, and the possibility of simultaneous operation.[17]

Microfluidic chips are made on the substrate of different materials such as glass, polymer, silicon, and paper. Paper is a low-cost substance to dispose of that is easy to make. Paper is made up of cellulose fibers, and the movement of fluid on these fibers is done by following the fibers, following the physics of capillarity and without the need for external force. The small thickness of paper reduces the use of reagents and solutions in conducting reactions, effective mixing in chemical experiments, reduction of reaction time, and better efficiency in response that take place on the paper.[18] The first μPAD appeared in 2007 from Whitesides' laboratory work and was created by a photolithography technique for the colorimetric detection of glucose in human urine samples.[19] Since then, μPADs have been used in many applications like medical, food safety, and forensic analysis.[20–22]

Contrary to lateral flow assays (LFAs) and dot tests, μPAD, flow samples, by way of the creation of flow channels, opened the door for multiplex detection in this type of device.[23] These channels are made using hydrophobic material and applying a pattern onto hydrophilic paper, thus defining the reaction zone through the creation of hydrophilic channels.[24] On two-dimensional (2D) μPADs, all channels are created by chemical or physical hydrophobic barriers through several techniques such as photolithography, wax printing, screen-printing, inkjet printing, and plasma oxidation, whereas three-dimensional (3D) μPADs are constructed by folding several layers of patterned paper.[21–26] For the construction of μPADs, the choice of fabrication technique should be done considering the cost, substrate used, fabrication time, and equipment availability.

μPADs only require very small amounts of fluids (nano to microliter) and provide faster responses than conventional laboratory techniques.[27] Furthermore, μPAD provides the advantage of miniaturization, disposability, and multiplex analysis by the creation of several channels and simultaneous semi-quantitative and quantitative responses.[21,24–28] These devices also allow on-site and on-demand analysis in real samples, which is an advantage for developing countries.[29] Despite all the advantages mentioned above and many efforts (including the use of pre-concentration techniques), μPADs can suffer from a lack of sensitivity. However, the commercialization of colorimetric sensors can be more affordable than other methods.[30] Anisotropic metal nanoparticles of various forms and sizes have piqued the curiosity of scientists.[31–33] Among them, silver and gold nanoparticles have drawn a lot of attention in recent years due to their unique optical properties and chromogenic characteristics.[34]

To date, various strategies have been used, based on changes in size, shape, and inter-particle distance for designing colorimetric chemosensors based on AgNPs and AuNPs.[35–38] In this regard, the aggregation–disaggregation approach has some drawbacks, including instability of bonded nanoparticles as well as unwanted effects of interferents in real samples.[39] There are also some compelling reasons for choosing AgNPs. The molar quiescence coefficient of AgNPs is roughly 100 times larger than that of AuNPs when compared at the same size, improving the perspectivity and sensitivity, subsequently.[40] Considering these issues, three types of AgNPs, such as silver nanoprism (AgNPrs), silver nanowires (AgNWs), and silver nanospheres (AgNSs), were synthesized in this work and applied for the optical detection of MDA in real samples. According to the obtained colorimetric results, AgNPrs were by far the best candidate to develop an MDA recognition system. From the previous studies, it is clear that AgNPrs possess platelike triangle shapes with wonderful electronic, optical, and structural properties. The LSPR for AgNPrs across visible-NIR regions is robust and any applied changes in vertex form, thickness, or edge length will alter its intensity.[41–45] Based on these facts, AgNPrs have a special place in the construction of colorimetric sensors.[46] So far, several sensors and biosensors have been developed by either etching or the growth of different analytes onto this optical nanoprobe.[31,47]

Recently, there has been a lot of interest in the integration of modern sensors on microfluidic substrates.[48] This is mainly because microfluidic systems offer a miniaturized automated

environment for the precise analysis of analytes in a micro-scale volume with time and cost efficiency.[49] A microfluidic paper-based colorimetric device (μPCD) is one of the most cost-effective open-droplet microfluidic systems, which can be readily made with minimal laboratory requirements.[46] Moreover, the instructions for preparing μPCD are straightforward and adjustable. In such systems, the lateral force caused by the nature of the paper will flow any injected solutions across the engulfed channels using hydrophobic materials like paraffin.[50] The last part of this study was devoted to the integration of the proposed colorimetric system into an optimized μPCD modified by AgNPrs for MDA analysis. In this study, AgNPrs due to their distinct color change were chosen for the optical recognition of MDA. In order to design an MDA colorimetric chemosensor based on AgNPrs and μPCD modified by AgNPrs, several colorimetric and spectrophotometric tests were conducted with the consideration of the reaction time. Notably, selectivity tests (combinative) with potential interferences were conducted and interpreted in full detail. Finally, an optimized way of producing μPCD for a readily absorbed solution like AgNPRs and a novel method for the rapid recognition of MDA was developed. For a better understanding, the procedure is summarized in Scheme 1.

2. Experimental

2.1. Chemicals and materials

Silver nitrate ($AgNO_3$), silver chloride (AgCl), PVP K-30 (polyvinyl pyrrolidone), sodium borohydride ($NaBH_4$, 96%), hydrogen peroxide (H_2O_2, 30 wt%), and tri-sodium citrate ($Na_3C_6H_5O_7$) were purchased from Sigma-Aldrich (Canada). Cysteine (Cys), aspartic acid (Asp), arginine (Arg), glucose (Glu), phenylalanine, tyrosine, methionine, proline, and glycine were obtained from Merck (Germany). MDA was obtained from Merck (Germany). The standard solutions of Na_2NO_3, K^+, Zn^{2+}, Mg^{2+}, and Ca^{2+} were provided by Chem Lab Company (Zedelgem, Belgium). All experiments were performed in compliance with the relevant laws and institutional guidelines

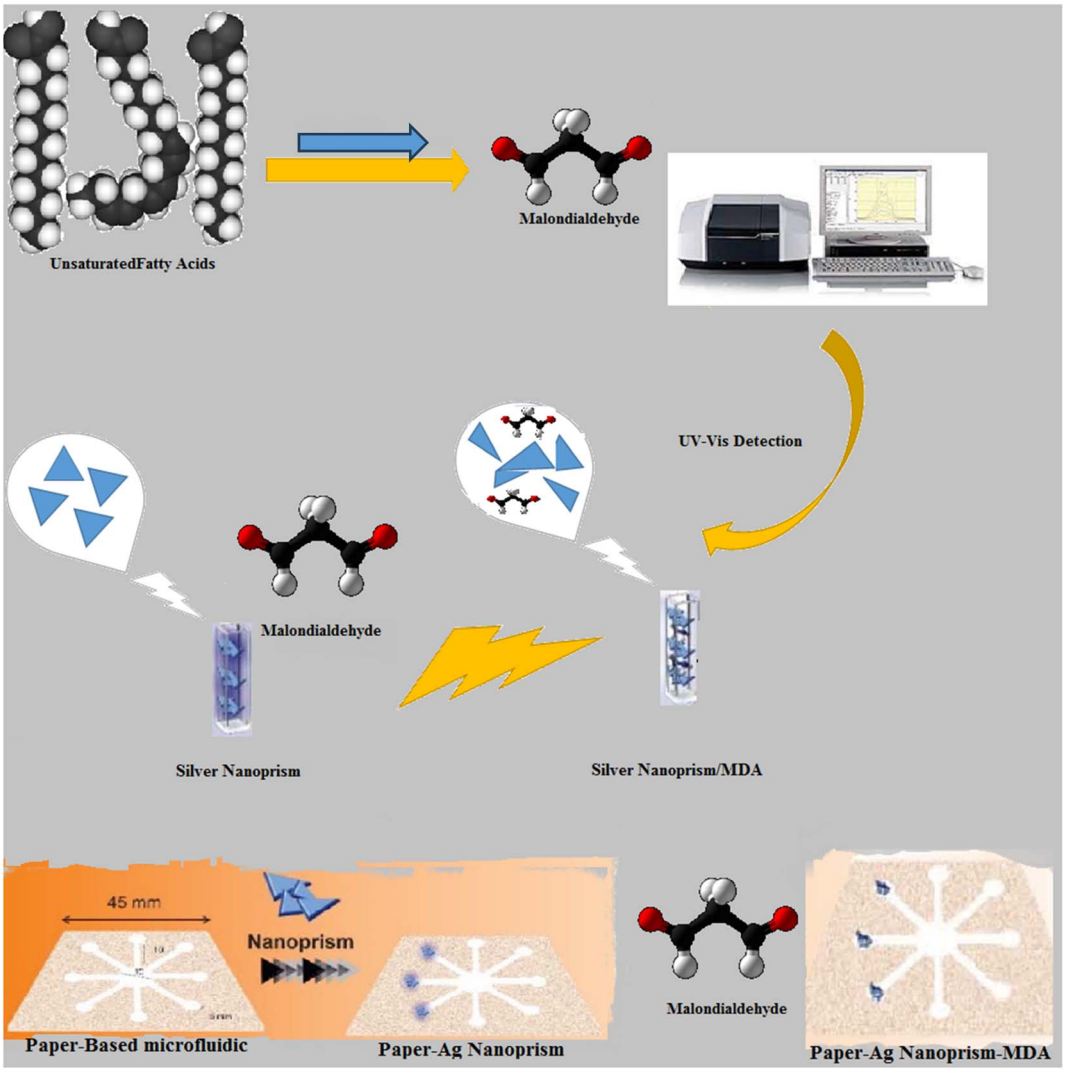

Scheme 1 Schematic illustration for the detection of MDA through UV-visible spectroscopy and OD-μPCD toward colorimetric assays.

(IR.TBZMED.VCR.REC.1402.010). This study was ethically approved by Tabriz University of Medical Sciences (Grant No. 71352).

2.2. Instrumentation

A Shimadzu UV-1800 UV-Vis spectrophotometer with 1 nm resolution was used to measure the absorbance. To analyze the size dispensation and recognize the zeta potential of the manufactured silver nanoparticles, we used Zetasizer Ver. 7.11 (Malvern Instruments Ltd, MAL1032660, England) for dynamic light scattering (DLS) analysis. For analysis, an EBC sample was collected from a healthy volunteer applying a lab-made device based on the invention registration Iranian cooling trap technique that the Iranian Patent Office patented. The created device can quickly condense exhaled air after breathing and offers a wide temperature range of 0 to 25 °C. All of the photographs and videos in this work were taken with a camera (Samsung Galaxy A2 Core smartphone). The images were recorded from natural light sources.

2.3. Synthesis and characterization of silver nanoprism (AgNPrs), silver nanospheres (AgNSs), and silver nanowires (AgNWs)

AgNPrs, AgNSs, and AgNWs were synthesized according to the previous project.[51] For the synthesis of AgNPrs, PVP was dissolved in water. Next, $AgNO_3$ was added to this solution and stirred. Then, under stirring condition, TSC and H_2O_2 was added to this solution. Finally, the reducing species ($NaBH_4$) was added to the above solution. The synthesis of AgNPrs was completed after 30 min under stirring condition. Finally, the colloidal solution was centrifuged at 6000 rpm for 15 min before being stored at 4 °C for later use.

For the synthesis of AgNSs, silver nitrate solution was mixed with TSC solution. Then, silver ions were reduced by the solution of $NaBH_4$. After 24 h stirring, the synthesis of AgNSs was completed.

For the synthesis of AgNWs, EG and PVP was stirred at 170 °C for 20–30 min. Then, AgCl solution was added to the previously prepared solution and stirred for 180 s at 107 °C. Next, $AgNO_3$ that was mixed with EG was added to the above-mentioned solution. Then, stirring was continued for 30 min at the same temperature. Finally, the prepared solution was centrifuged for 30 min at 6000 rpm, which led to the completion of the synthesis process of AgNWs.

2.4. Preparation of real samples

Condensation of exhaled breath is a possible approach to measure and analyze compounds in the airway lining fluid.[52] There are several different commercial devices for sampling by different commercial companies. The basis of all of them is the rapid cooling of exhaled breath (Scheme S1 (see ESI†)). A schematic illustration of the workmanship of breath aerosol formation in a bronchiole and the basic components of the EBC collection devices are shown. EBC samples must be collected during normal resting tidal breathing (RTB) of subjects at room temperature; the small droplets of the lung lining fluid and breathing water vapor are condensed to a liquid or solid phase depending on the condenser of temperature. Temperature is a powerful stimulant for controlling salivary DNase activity; thus, EBC samples should be kept on ice immediately, then frozen was stored at or below −20 °C until extraction However, the importance of the proper selection of the sampling device is not negligible because it has been proved that the sampling temperature and coating material of the sample collection tube—silicone, glass, aluminum, polypropylene, and Teflon—can affect the biomarkers' concentration in EBC. In this work for analysis, an EBC sample was collected from a healthy volunteer applying a lab-made device based on the invention registration Iranian cooling trap technique that the Iranian Patent Office patented (Patent No. 81363). EBC samples prepared from a healthy volunteer were transferred to a 0.1 mL volumetric flask, a standard solution with the requested concentration was added up to the marked line, and spectrophotometric analysis was performed. Also, to evaluate the effect of AgNPrs and MDA in the real sample, a healthy urine sample was used without any pretreatment.[53]

3. Paper-based microfluidic device fabrication

In this work, to evaluate the efficiency of papers, fiberglass and TLC paper were used; the results showed that fiberglass paper has less attrition due to better flow. Paraffin was used because of its benefits, including its low melting point, inexpensive cost, and thermoplastic characteristics. Furthermore, paraffin, a key ingredient in solid, is frequently employed in the production of μPCDs in the wax printing method and is resistant to the majority of the chemical compounds used in the study. Standard μPADs were constructed *via* wax printing.[54,55] The proposed pattern consists of eight hydrophilic circular zones. The prepared paper-based template has micro-channels that have a capillary low, and the liquid can pass through it easily. The designed microfluid can analyze several samples simultaneously. This work is melted at a temperature of 90 °C and then the appropriate paper is floated in it for 30 s. After drying, the iron pattern was heated for two min at 150 °C. Between the iron design and the magnet, a sheet of paper was placed. As a result, the paraffin penetrated into the paper's structure and formed hydrophilic channels on the surface. The prepared μPCD after drying was utilized for colorimetric analyses (Scheme S2 (see ESI†)). MDA was discovered using μPCD modified by optical nanoprobes (AgNPrs and AgNWs). For the decoration of detection zones, one droplet of probes was immobilized and dried at room temperature. Therefore, the suggested method is a step toward the creation of MDA diagnostic kits that are qualitatively superior and can change color quickly and inexpensively. As a result, the paraffin penetrated into the paper's structure and formed hydrophilic channels on the surface. The prepared μPCD after drying was utilized for colorimetric analyses (Scheme S2 (see ESI†)).

4. Results and discussion

4.1. Identifying appropriate type of AgNPs for MDA detection colorimetric assay

Three different AgNPs, namely, AgNPrs, AgNSs, and AgNWs, were synthesized and mixed with 5.90 mM MDA standard solution at a 1 : 1 v/v ratio to induce distinct color changes for analyte detection. As shown in (Fig. S1 (see ESI†)), there is a clear color change for AgNPrs. Also, after adding MDA to AgNPrs, its color changed from sea blue to purple. Interestingly, after 1 h, the color of the mixture had changed to yellowish gray. The combination of AgNSs aqueous solution and MDA showed colorless change, while the AgNWs showed no color after mixing with MDA. Accordingly, AgNPrs were selected for further investigation.

4.2. Confirmation of MDA reaction with nanoprobe using color change, UV-Vis method

UV-Vis spectra of AgNPrs, MDA, and AgNPrs after the addition of MDA at different incubation times were recorded and are shown in Fig. 1. As can be seen, for AgNPrs, LSPR peaks were obtained at 571 and 575 nm for 0 (immediately) and 60 min, respectively. By spiking the AgNPrs solution with MDA, the intensity of the UV/Vis peaks decreased significantly. The greatest shift for this band appeared at 566 nm after 60 min.

Triangular AgNPrs have an extraordinary degree of anisotropy and show one of a kind LSPR highlights with a tall termination coefficient. Upon the expansion of MDA, the morphology of these triangular AgNPrs changed to circular nanodisks and the color changed from blue to yellow, depending on the degree of carving. Moreover, the UV-Vis spectra of the triangular AgNPrs display wide highlights with three unmistakable groups at 335 nm, 475 nm, and 750 nm, which are attributed to the out-of-plane quadrupole, in-plane quadrupole, and in-plane dipole plasmon reverberation of the triangular AgNPrs, respectively. The in-dipole reverberation top at 750 nm is highly sensitive to the thickness and edge length of triangular AgNPrs. As anticipated, the wide crest at 750 nm, attributed to the in-plane dipole reverberation, vanished taking after the expansion of MDA, whereas the top at 480–500 nm was slowly expanded (Fig. 1), which demonstrate that the location of MDA with this triangular AgNPrs test is highly sensitive to the nanoprism shape *versus* the top position of the in-plane dipole reverberation.

4.3. Analytical study

To study the concentration effect of MDA by colorimetric and spectroscopic methods, various concentrations of MDA (0.01192 to 1.192 mM) were prepared in deionized water. Then, AgNPrs were added to MDA solution in a 1 : 1 v/v ratio. These mixtures were photographed in different incubation times [0, 30, and 60 min]. As can be seen in Fig. 2, the color of MDA at different times (0, 60 min) were changed to taupe and a brighter shade, especially after some seconds had passed, for 0.01192 to 1.192 mM concentrations of MDA. The results show that the effect of MDA on the color of AgNPrs not only depends on its concentration but that the reaction time is also a key factor. The reason of this approach is related to different changes in the morphology of AgNPrs in the presence of different concentrations of MDA at various incubation times. The three absorption bands can be assigned to out-of-plane and in-plane quadrupole resonance and in-plane dipole resonance of AgNPrs, respectively. Furthermore, the peak of the in-plane dipole resonance is highly shape dependent, which is utilized to design wavelength alterations-based sensors. With the addition of MDA, a blue shift in the in-plane dipole resonance peak in the LSPR spectra

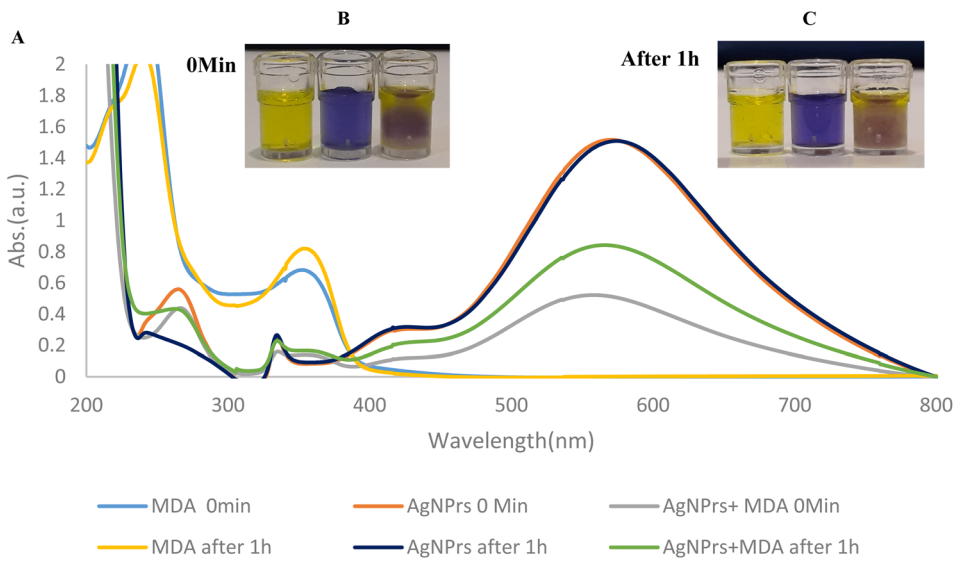

Fig. 1 (A) UV-Vis absorption spectra of AgNPrs, AgNPrs + MDA (5.90 and 10 mM), at different incubation times [0 min and after 1 h], (B) photographic images of AgNPrs, AgNPrs + MDA (5.90 mM, 10 mM), at the first incubation time [0 min] with the nanoprobe. (C) Photographic images of AgNPrs, AgNPrs + MDA (5.90 and 10 mM) after 60 min incubation with the nanoprobe.

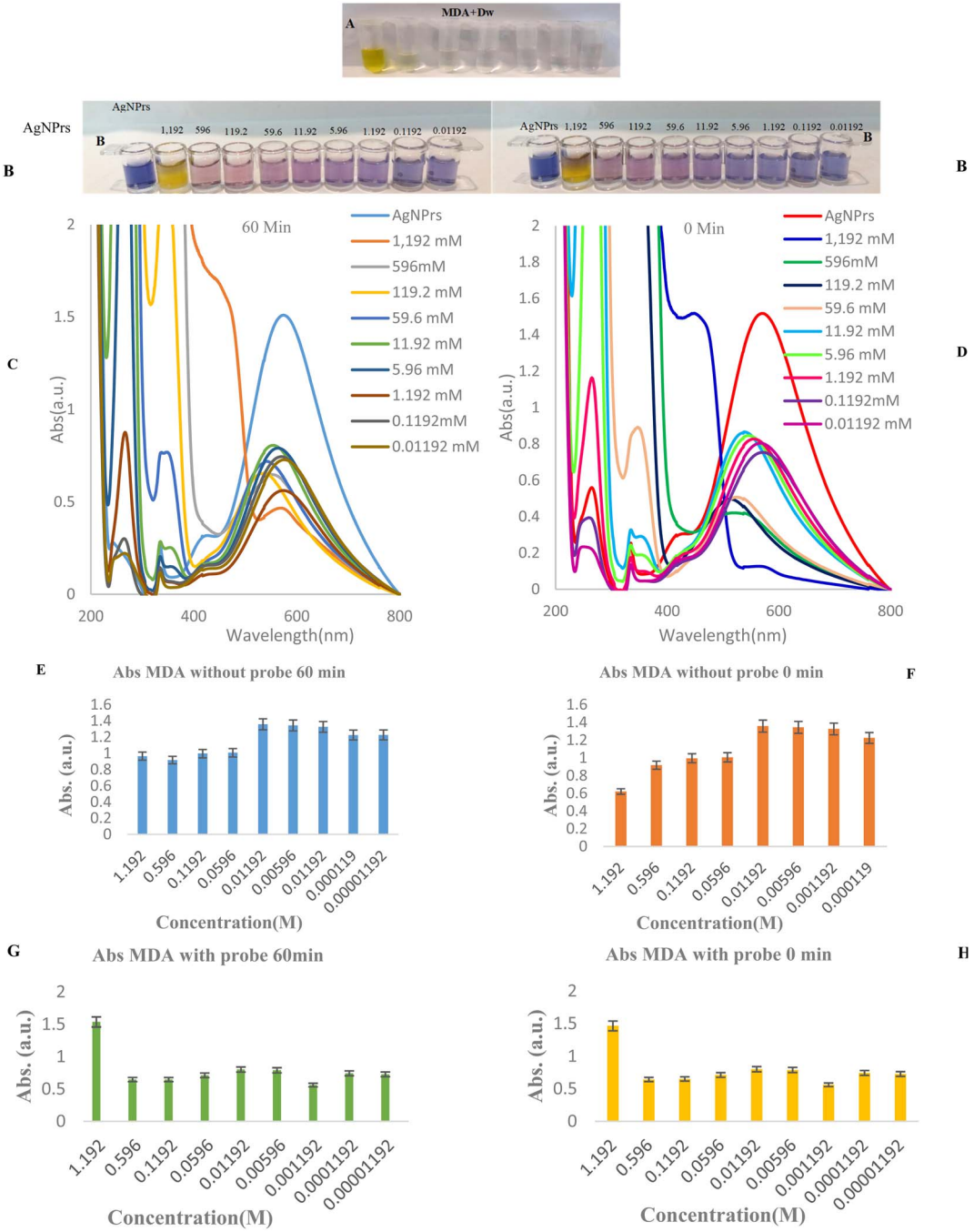

Fig. 2 (A) Digital photos of MDA with deionized water of various concentrations. (B) Colorimetric sensing of AgNPrs spiked with various concentrations of MDA at two different incubation times (0 and 60 min), (C) UV-Vis spectra of different concentrations of MDA with AgNPrs at a 1 : 1 v/v ratio in 60 min. (D) The UV-Vis spectra of different concentrations of MDA with AgNPrs at a 1 : 1 v/v ratio in 0 min. (E) The histogram curve of peak intensity *versus* MDA concentration without probe from 0.01192 to 1.192 mM after 60 min incubation with a nanoprobe. (F) The histogram curve of peak intensity *versus* MDA concentration without the probe from 0.01192 to 1.192 mM in the first incubation time [0 min]. (G) A histogram curve of peak intensity *versus* MDA concentration with the probe from 0.01192 to 1.192 mM at the first incubation time [0 min]. (H) A histogram curve of peak intensity *versus* MDA concentration with the probe from 0.01192 to 1.192 mM after 60 min incubation with the nanoprobe.

and color change of the solution from blue to yellow was observed. These phenomena are attributed to the morphology transformation of AgNPrs and the tendency of newly generated Ag atoms to deposit on the surface of AgNPrs. Thus, the wavelength shift of the in-plane dipole resonance peak of AgNPrs was used for the determination of MDA. Based on this result, a minimum concentration of 0.01192 mM MDA in a standard solution could be easily detected by the naked-eye

(Fig. 2). The second part of this study was allocated to the utilization of UV-Vis spectra at different concentrations and various incubation times. As shown in Fig. 2, MDA with concentrations in the range from 0.01192 to 1.192 mM has the capability of shifting the spectrum of the absorption band using calibration curves, causing a change in the solution color from dark violet to pink. Subsequently, the regression equation of $y = -11.3 \ln(C_{MDA}) + 624.43$, $R^2 = 0.846$ and $y = -8.133 \ln(C_{MDA}) + 682.9$, $R^2 = 0.8096$ were achieved at 0 and 60 min (incubation time), which confirmed the linear relationship between wavelength and concentration in this concentration range. Furthermore, the absorbance band was in a linear relationship with MDA concentrations over the ranges 0.01192 to 1.192 mM and 1.192 to 5.96 mM with regression equations of Abs (MDA) of $y = -0.552C_{(MDA)} + 1.2696$, $R^2 = 0.8305$ from 0.01192 mM to 1.192 mM concentrations and $y = -0.01242C_{(MDA)} + 1.045$, $R^2 = 0.842$ for 1.192 to 5.96 mM was also obtained, which confirms the downward trend of the absorption band in relation to the Napierian logarithm of MDA concentration. Based on the acquired data, the suggested colorimetric spectrophotometric measurement assays based on AgNPrs has linear range of 0.01192 to 1.192 mM and 1.192 to 5.96 mM, respectively. It is obvious that the absorption bands of the spectrum decreased with the increase in MDA concentration. The results indicate that the efficient interaction of MDA with AgNPrs depends not only on its concentration but also on the response time.

In Table 1,[54-61] the analytical performances of various methods for the detection of MDA including surface-enhanced Raman spectroscopy (SERS), fluorescence spectroscopy electropolymerization, UV-Vis, fluorescence, and electrochemical sensing, have been compared.

The majority of the reported techniques have various advantages, including low sensitivity, complicate mobile phases, and time-consuming extraction procedures with restricted applicability. A comparison of the results obtained in this study with previously reported works (Table 1) shows that the developed method shows some advantages over previous approaches, stability, suitable surface area, and feasible biological activity. The strong points of our study include the use of the calorimetric chemosensing procedure for the determination of MDA in urine samples for the first time. We believe that the designed approach is a good bio-assay for determining MDA quantitatively in real samples. In terms of response, the proposed chemosensor approach clearly outperforms previously reported methods.

4.4. Real sample analysis

The reported colorimetric and spectrophotometric approaches were also utilized to detect MDA in human urine samples. Based on the results acquired, MDA in the urine sample was mixed with AgNPrs in a 1 : 1 v/v ratio and 1 : 0.5 : 0.5 v/v/v ratio. Then, they were analyzed by colorimetric and UV/Vis methods. As shown in Fig. 3, after 60 min, the color of the mixture was changed to brighter blue.

Higher levels of MDA, in human biofluids like EBC, serum, and plasma, have been observed in subjects with diseases characterized by oxidative stress, such as respiratory, diabetes, cardiovascular, and cancer. But, according to the results obtained in Fig. S2 (see ESI†), the AgNPrs probe does not have the ability to identify MDA in EBC samples. This is related to matrices of real samples (EBC) and maybe the low concentration of MDA at this biofluid. On the other hand, MDA is easily deprotonated to give the sodium salt of the enolate. In neutral solution, MDA is present as the relatively unreactive enolate anion or at lower pH as the β-hydroxyacrolein and can thus form adduct by Michael addition and Schiff base formation. Under physiological conditions, MDA reacts primarily with the ε-amino groups of protein lysine residues and has been observed to cause protein cross-linking. MDA can form adducts with both proteins and DNA and has been shown to form DNA adducts

Table 1 Analytical figure of merit of various detection methods of MDA

Method	Nanoprobe, nanopolymer	LOD/LOQ/LLOQ	Samples	Ref.
SERS	4-Aminothiophenol (4-ATP)-modified Au nanoflowers (Au NFs) probes	$\sim 3.6 \times 10^{-13}$ M	Human serum	54
Fluorescence spectroscopy	MDA (MDAP-1)	0.6 mM	Living cell	55
Fluorescence spectroscopy	(Mito-FMP) based on a benzoxadiazole platform	Not reported	Hela cells	56
Electropolymerization	PARG-GQDs-CS	5.94 nM	Breath samples	57
Spectrophotometric	DES smart labels	Not reported	Real samples (fried seed oil)	58
SERS	4-Aminophenylthiophenol (PATP)	0.50 μM	Blood samples	59
UV-Vis/fluorescence	4-Hydrazinyl-7-nitrobenzofurazan (NBDH)	The MDA detection range of our probe NBDH falls between 0.1 and 20 μM, and the corresponding detection limit amounts to 7.2 nM	Serum samples	60
Electrochemical sensing	Polymer (MGO@MIPy)	0.01 μM	Chicken serum samples	61
Colorimetric and spectrophotometric chemosensor	AgNPrs probe	0.12 μM	Urine, EBC	This work

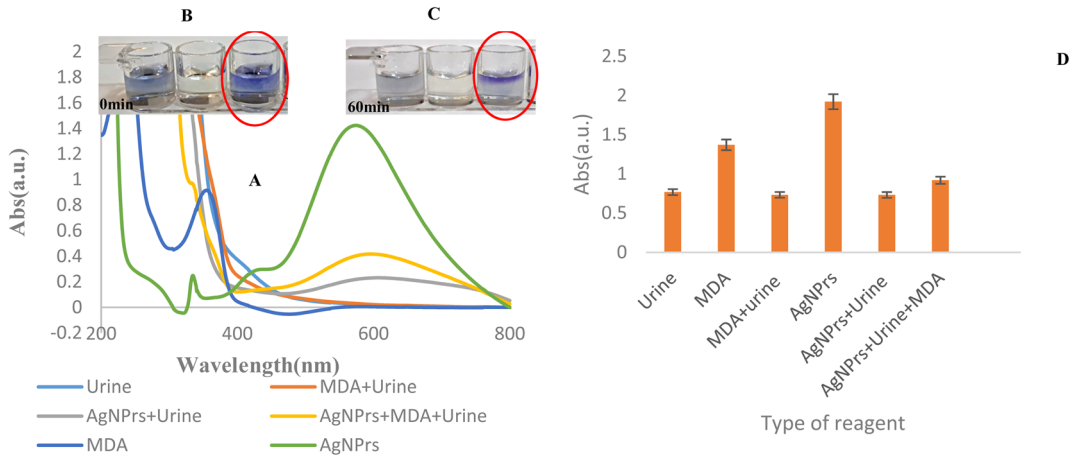

Fig. 3 (A) UV-Vis spectra, urine, urine + AgNPrs, MDA, MDA + urine, AgNPrs, AgNPrs + MDA + urine a 1 : 1 v/v ratio and 1 : 0.5 : 0.5 v/v/v ratio. (B) Photographic images of urine, urine + AgNPrs, MDA, MDA + urine, AgNPrs, AgNPrs + MDA + urine a 1 : 1 v/v ratio and 1 : 0.5 : 0.5 ratio in 0 min. (C) Photographic images of urine, urine + AgNPrs, MDA, MDA + urine, AgNPrs, AgNPrs + MDA + urine in 1 : 1 ratio and 1 : 0.5 : 0.5 v/v/v ratio in 60 min. (D) The histogram curve of peak intensity, urine, urine + AgNPrs, MDA, MDA + urine, AgNPrs, AgNPrs + MDA + urine.

even in the human liver devoid of any overt disease. So, it seems that the determination of MDA in EBC samples needs a pre-concentration process before measurement.

4.5. Selectivity analysis

Considering the fact that the selectivity is one of the important aspects of biomedical analysis, it was evaluated by performing the assessment in the presence of other species in real samples. For this purpose, 10 mM solutions of Na_2NO_3, Mg^{2+}, Zn^{2+}, Ca^{2+}, K^+, glycine (Gly), tyrosine (Tyr), cysteine (Cys), aspartic acid (Asp), arginine (Arg), phenylalanine (phenyl), methionine (Met), proline (Pro), and glucose (Glu) were mixed with AgNPrs solution in 1 : 1 v/v ratio, and the results of colorimetric and UV/Vis spectra were compared with an MDA/AgNPrs mixture under the same conditions to detect any resemblance to an MDA effect. Since the etching effect of MDA and other similar species on AgNPrs depends on the reaction time, the time for examination was set to 0 and 60 min after mixing the components. While other mixtures changed the color to a lighter shade, the obtained data revealed the suitable selectivity of AgNPrs as an optical probe toward interaction with MDA in the first minute of the reaction. In the second step, 50 μL MDA (10 mM, the minimum required concentration of MDA for shifting the color of the AgNPrs to violet) was combined with 50 μL interferential species (10 mM). Then, 100 μL AgNPrs was added to the MDA/interference mixture, and colorimetric/spectrophotometric study was done. At the same initial moment, since the addition of metal ions, the blue color of AgNPrs changed to yellow, and the amino acid cysteine changed color. But the amino acids tyrosine, phenylalanine, arginine, and glucose affect the color of the optical probe at 0 min immediately after interaction, but after 60 min incubation of the optical probe for analytical analysis, the color became lighter. But the amino acids methionine, aspartic acid, and proline appeared with a dark purple color at first and changed to a pale purple color after 60 min (Fig. S3 (see ESI†)). According to the obtained results of metal ions and amino acids, these species alone cannot significantly interact with MDA in the measured amounts. Therefore, these species have no interfering effect on the performance of the MDA photochemical sensor (Fig. S4–S11) (see ESI†). But with the addition of the probe (AgNPrs) to the desired composition and the effect of the interaction between the probe and the desired analyte in the presence of interferers, it shows that these species have a similar structure to the analyte candidate (MDA) and cannot bind to the probe and cause interference.

4.6. Stability

The colloidal stability of MDA solution was tested for 3 days with different concentrations (high (596 mM), medium (11.92 mM), low (0.1192 mM)) of MDA solution at 0 and 60 min, and the results were reported as standard deviation (SD). As shown in Fig. S12 (see ESI†), the result obtained from the UV-Vis spectrum shows no significant changes in the three absorption bands. Although the intensity of the absorption bands decreased gradually, the decrease ratio was almost the same for all the absorption bands without affecting the wavelength position, which shows the great reproducibility of the method. So, the results show that the tests are approved and the created platform is completely stable. One of the most important advantages of an ideal biosensor is its high stability.

4.7. Naked-eye colorimetric MDA analysis using one-droplet paper-based microfluidic system

4.7.1. Integration of the colorimetric recognition system with microfluidic paper. To integrate the colorimetric MDA analysis system with μPAD paper, two kinds of microfluidic papers were prepared and underwent examination. In the first attempt, the microfluidic network was established with 20 s of heat and pressure on the fiberglass paper. The hydrophilic network of the prepared microfluidic paper was very permeable toward AgNPrs and MDA. As soon as AgNPrs and MDA were

injected, they were absorbed in the paper. So, no noticeable color change occurred in the injected areas' protection zone. In a second attempt, the time of exposure to molten paraffin was increased to 30 s subsequently and the hydrophilic network changed to a semihydrophobic one, which was more resistant to the absorption of AgNPrs and MDA. As a result, the injected drop of AgNPrs and MDA took almost 30 min of reaction time until they either were absorbed into the paper or dried (Fig. S13 and S14 (see ESI†)). This alteration in the preparation of the microfluidic paper made it suitable for AgNPr-based colorimetric systems based on a time/color shift system (see Video (see ESI†)).

4.7.2. Analytical approach. For the analytical study using the constructed μPCD colorimetric chemosensor (Fig. 4), wells no. 2 to no. 8 were injected with 5 mL of different concentrations of MDA (1.192, 596, 119.2, 59.6, 5.96, 11.92, 0.12, 0.06, 0.012, 0.006, 0.0012, 0.0006, 0.00012 mM). 5 min after adding 5 mL of freshly prepared AgNPrs into all wells from no. 2 to no. 8, the color change was evident at 1.192, 596, 119.2, 59.6, and 5.96 mM concentrations of MDA for the incubation of the probe with MDA on the surface of μPCD. After 15 min of reaction time, 1.192, 596, 119.2, 59.6, 5.96, 11.92, and 0.12 mM MDA concentration experienced a color change to orange, and 0.06 mM MDA concentration (change to purple) and other concentrations of MDA remained blue in color. After 45 min, the color of the zones with high concentration of MDA [1.192, 596, 119.2, 59.6, 5.96, 11.92, 0.12, and 0.06 mM] was changed. But the low concentrations still remained blue during this period (see Video (see ESI†)).

4.7.3. Selectivity analysis using the OD-μPCD system. To investigate the effect of the possible interfering of other species on MDA measurement, the interaction of AgNPrs as the optical probe with ten types of potential interferers [glycine (Gly), tyrosine (Tyr), cysteine (Cys), aspartic acid (Asp), arginine (Arg), phenylalanine (phenyl), methionine (Met), proline (Pro)] in 1 : 0.5 : 0.5 v/v ratio at a concentration of 10 mM were evaluated using OD-μPCD. In practice, in the initial examination (Fig. S15 (see ESI†)) at different times, 10 μL AgNPrs was injected into each well of OD-μPCD from no. 1 to no. 8. Afterward, 5 μL MDA [0.001 M] was added to wells no. 2 to no. 8. After 5 min, the color change of the well containing the interferer cysteine changed noticeably, while the other wells did not show any noticeable change. After 30 min, the hue of some of the wells also changed, which was related to proline and methionine interferences. After 1 h, in addition to proline and methionine, glycine also showed a very noticeable color change. Well no. 3, 5, 6 (D1), and 4 (D2) containing arginine, phenylalanine, tyrosine, and aspartic acid, respectively, did not color change of the zones significantly. The obtained results indicate that none of these species can interfere with MDA at the same concentration. Nevertheless, at concentrations of 10 mM proline, glycine turned the hue of AgNPrs to pink after 1 h, which can be considered an interferer in the performance of chemosensor on the recognition of MDA. However, we also investigated the interactions separately for MDA and AgNPrs and recorded the

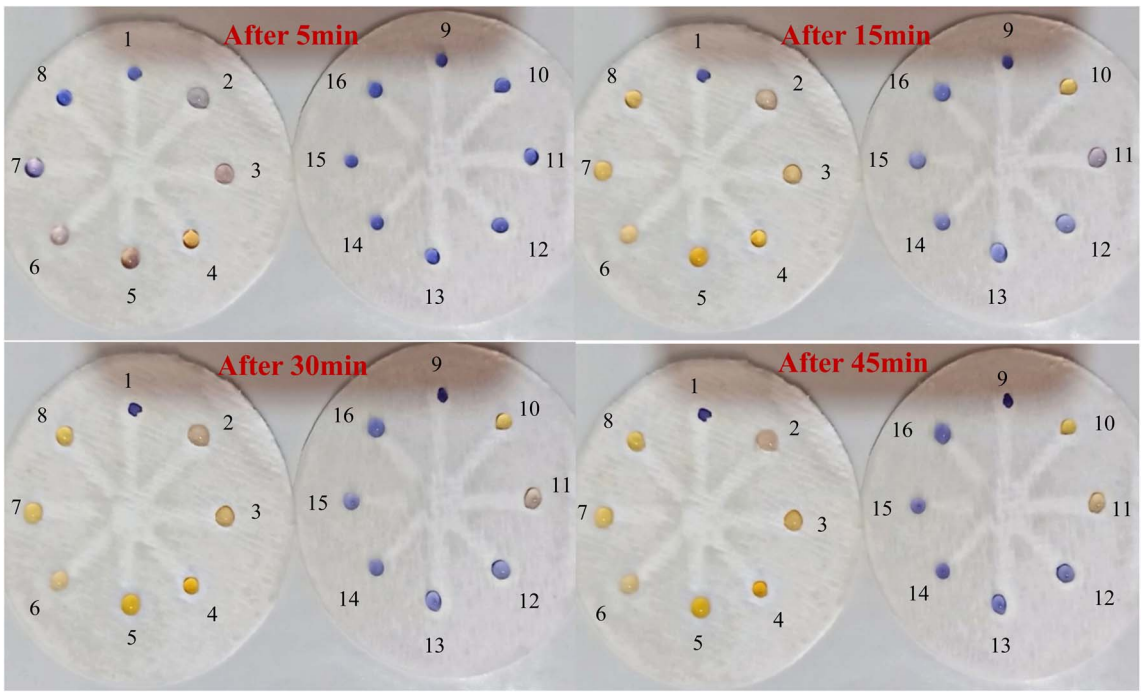

Fig. 4 Photographic images of the fiberglass microfluidic paper-based colorimetric chemosensor, without and with different concentrations of MDA at different reaction times. (1) AgNPrs without MDA, (2) MDA, (3) AgNPrs, 1.192 mM MDA, (4) AgNPrs, 596 mM MDA, (5) AgNPrs, 119.2 mM MDA, (6) AgNPrs, 59.6 mM MDA, (7) AgNPrs, 5.96 mM MDA, (8) AgNPrs, 11.92 mM MDA, (9) AgNPrs without MDA, (10) AgNPrs, 0.12 mM MDA (11) AgNPrs, 0.06 mM MDA, (12) AgNPrs, 0.012 mM MDA, (13) AgNPrs, 0.006 mM MDA, (14) AgNPrs, 0.0012 mM MDA, (15) AgNPrs, 0.0006 mM MDA, and (16) AgNPrs, 0.00012 mM MDA.

results for different times. As shown in Fig. S16 and S17 (see ESI†), at different incubation times, no color changes occurred. Therefore, it was concluded that when interferons are combined with AgNPrs and combined with MDA, they lead to interaction (see Video (see ESI†)).

5. Conclusions

In this study, three different types of AgNPrs, AgNSs, and AgNWs were evaluated for the recognition of MDA in human biofluids. Since AgNPrs showed excellent colorimetric spectrophotometric results, they underwent thorough examination. The obtained analytical results of the designed colorimetric chemosensor are comparable with other reports as this sensing system enjoys a linear range of 0.00012–1.192 mM with an LLOQ of 0.00012 mM. Moreover, AgNPrs could successfully detect MDA in human urine sample. In the last part of this work, a reported OD-μPCD was optimized for integration with the colorimetric system. This optimization paved the way for offering an innovative analytical strategy that is based on the time/color characterization of each concentration of MDA with suitable selectivity. The selectivity tests for the one-droplet microfluidic systems were also appropriate. Also, the stability of the AgNPrs was confirmed for at least 30 days, which makes the commercialization of the proposed system more achievable. What this study offers, apart from the simple and sensitive colorimetric recognition system for MDA, is an optimized OD-μPCD as a suitable substrate for solutions like AgNPrs that are readily absorbable by paper and a creative time/color system for obtaining a rough estimation of the analyte concentration. The results revealed that the presented paper-based microchips can detect MDA and can be developed to provide on-site diagnostic kits. In addition to the simple, rapid, sensitive colorimetric and spectrophotometric and OD-μPCD recognition system of malondialdehyde, this study provides a novel portable platform for the monitoring of MDA in real samples. The proposed system had better selectivity and lead to high sensitivity of the bioassay. As a result, we expect that the designed platform will provide a new horizon for the sensitive measurement of MDA in spiked samples. Indeed, because of their advantages, such as simple tool, rapidness, excellent compatibility with miniaturized technologies, and remarkable sensitivity to the target, calorimetric chemosensing-based methods have more applications compared to other sensing technologies. The obtained results of metal ions and amino acids show that these species alone cannot significantly interact with MDA in the measured amounts. Therefore, these species have no interfering effect on the performance of the MDA photochemical sensor. But with the addition of the probe (AgNPrs) to the desired composition and the effect of the interaction between the probe and the desired analyte in the presence of interferers, it shows that these species have a similar structure to the analyte candidate (MDA) and cannot bind to the probe and cause interference. It is important to point out that the selectivity of the present platform should be improved. Also, the proposed chemo-probe stability should be improved using some stabilizers. Finally, the application of the proposed sensor for the validated monitoring of human biofluids should be improved in the next studies.

Conflicts of interest

There are no conflicts to declare.

Acknowledgements

We are grateful for financial assistance for this work from the Research Center for Pharmaceutical Nanotechnology, Tabriz University of Medical (Grant No. 71352)-(IR.TBZMED.VCR.REC.1402.010).

References

1 N. Ratcliffe, T. Wieczorek, N. Drabińska, O. Gould, A. Osborne and B. D. L. Costello, A mechanistic study and review of volatile products from peroxidation of unsaturated fatty acids: an aid to understanding the origins of volatile organic compounds from the human body, *J. Breath Res.*, 2020, **14**, 034001.

2 M. Repetto, J. Semprine and A. Boveris, Lipid peroxidation: chemical mechanism, biological implications and analytical determination, *Lipid Peroxid.*, 2012, **1**, 3–30.

3 M. A. Babizhayev, The detox strategy in smoking comprising nutraceutical formulas of non-hydrolyzed carnosine or carcinine used to protect human health, *Hum. Exp. Toxicol.*, 2014, **33**, 284–316.

4 A. M. Pisoschi and A. Pop, The role of antioxidants in the chemistry of oxidative stress: a review, *Eur. J. Med. Chem.*, 2015, **97**, 55–74.

5 S. K. Jain, R. McVIE and T. Smith, Vitamin E supplementation restores glutathione and malondialdehyde to normal concentrations in erythrocytes of type 1 diabetic children, *Diabetes Care*, 2000, **23**, 1389–1394.

6 D. Bencivenga, F. Arcadio, A. Piccirillo, M. Annunziata, F. Della Ragione, N. Cennamo, A. Borriello, L. Zeni and L. Guida, Plasmonic optical fiber biosensor development for point-of-care detection of malondialdehyde as a biomarker of oxidative stress, *Free Radicals Biol. Med.*, 2023, **199**, 177–188.

7 T. Zhang, J. Pei, X. Li, H. Li and F. Inscore, A surface-enhanced Raman sensor for trace identification and analysis of high-priority drugs of abuse with portable and handheld Raman devices, *J. Raman Spectrosc.*, 2022, **53**, 1494–1514.

8 L. Ju, A. Lyu, H. Hao, W. Shen and H. Cui, Deep learning-assisted three-dimensional fluorescence difference spectroscopy for identification and semiquantification of illicit drugs in biofluids, *Anal. Chem.*, 2019, **91**, 9343–9347.

9 R. Y. Luo, C. Wong, J. Q. Xia, B. E. Glader, R.-Z. Shi and J. L. Zehnder, Neutral-Coating Capillary Electrophoresis Coupled with High-Resolution Mass Spectrometry for Top-Down Identification of Hemoglobin Variants, *Clin. Chem.*, 2023, **69**, 56–67.

10 W. Łuczaj, M. Biernacki, I. Jarocka-Karpowicz and E. Skrzydlewska, Analytical Approaches to Assessment of Phospholipid Metabolism in Physiology and Pathology, *Handbook of Bioanalytics*, Springer, 2022, pp. 1–26.

11 W.-C. Tian and E. Finehout, Microfluidic diagnostic systems for the rapid detection and quantification of pathogens, *Microfluidics for Biological Applications*, 2009, pp. 271–322.

12 G. Bhattacharjee, R. Maurya, K. J. Alzahrani, N. Gohil, N. L. Lam and V. Singh, Microfluidics based point-of-care for disease diagnostics, *Prog. Mol. Biol. Transl. Sci.*, 2022, **187**, 241–248.

13 A. E. Ongaro, Z. Ndlovu, E. Sollier, C. Otieno, P. Ondoa, A. Street and M. Kersaudy-Kerhoas, Engineering a sustainable future for point-of-care diagnostics and single-use microfluidic devices, *Lab Chip*, 2022, **22**, 3122–3137.

14 N. Kumar, M. Kumari and R. K. Arun, Development and Implementation of Portable Biosensors in Microfluidic Point-of-Care Devices for Pathogen Detection, *Miniaturized Biosensing Devices: Fabrication and Applications*, Springer, 2022, pp. 99–122.

15 D. Gao, H. Liu, Y. Jiang and J.-M. Lin, Recent developments in microfluidic devices for *in vitro* cell culture for cell-biology research, *TrAC, Trends Anal. Chem.*, 2012, **35**, 150–164.

16 A. E. Herr, A. V. Hatch, W. V. Giannobile, D. J. Throckmorton, H. M. Tran, J. S. Brennan and A. K. Singh, Integrated microfluidic platform for oral diagnostics, *Ann. N. Y. Acad. Sci.*, 2007, **1098**, 362–374.

17 S. Sohrabi and M. K. Moraveji, Droplet microfluidics: fundamentals and its advanced applications, *RSC Adv.*, 2020, **10**, 27560–27574.

18 M. O. Dillioglugil, H. Mekık, B. Muezzinoglu, T. A. Ozkan, C. G. Demir and O. Dillioglugil, Blood and tissue nitric oxide and malondialdehyde are prognostic indicators of localized prostate cancer, *Int. Urol. Nephrol.*, 2012, **44**, 1691–1696.

19 A. W. Martinez, S. T. Phillips, M. J. Butte and G. M. Whitesides, Patterned paper as a platform for inexpensive, low-volume, portable bioassays, *Angew. Chem.*, 2007, **119**, 1340–1342.

20 K. Yamada, H. Shibata, K. Suzuki and D. Citterio, Toward practical application of paper-based microfluidics for medical diagnostics: state-of-the-art and challenges, *Lab Chip*, 2017, **17**, 1206–1249.

21 T. Ozer, C. McMahon and C. S. Henry, Advances in paper-based analytical devices, *Annu. Rev. Anal. Chem.*, 2020, **13**, 85–109.

22 W. Alahmad, A. Sahragard and P. Varanusupakul, Online and offline preconcentration techniques on paper-based analytical devices for ultrasensitive chemical and biochemical analysis: a review, *Biosens. Bioelectron.*, 2021, **194**, 113574.

23 C. Carrell, A. Kava, M. Nguyen, R. Menger, Z. Munshi, Z. Call, M. Nussbaum and C. Henry, Beyond the lateral flow assay: a review of paper-based microfluidics, *Microelectron. Eng.*, 2019, **206**, 45–54.

24 W. Y. Lim, B. T. Goh and S. M. Khor, Microfluidic paper-based analytical devices for potential use in quantitative and direct detection of disease biomarkers in clinical analysis, *J. Chromatogr. B*, 2017, **1060**, 424–442.

25 L. Liu, D. Yang and G. Liu, Signal amplification strategies for paper-based analytical devices, *Biosens. Bioelectron.*, 2019, **136**, 60–75.

26 K. Wang, J. Yang, H. Xu, B. Cao, Q. Qin, X. Liao, Y. Wo, Q. Jin and D. Cui, Smartphone-imaged multilayered paper-based analytical device for colorimetric analysis of carcinoembryonic antigen, *Anal. Bioanal. Chem.*, 2020, **412**, 2517–2528.

27 Y. Wu, Q. Gao, J. Nie, J.-z. Fu and Y. He, From microfluidic paper-based analytical devices to paper-based biofluidics with integrated continuous perfusion, *ACS Biomater. Sci. Eng.*, 2017, **3**, 601–607.

28 T. Ming, J. Luo, J. Liu, S. Sun, Y. Xing, H. Wang, G. Xiao, Y. Deng, Y. Cheng and Z. Yang, Based microfluidic aptasensors, *Biosens. Bioelectron.*, 2020, **170**, 112649.

29 Z. Sun, Y. Sun, M. Yang, H. Jin and R. Gui, A petal-shaped MOF assembled with a gold nanocage and urate oxidase used as an artificial enzyme nanohybrid for tandem catalysis and dual-channel biosensing, *Nanoscale*, 2021, **13**, 13014–13023.

30 G. M. Fernandes, W. R. Silva, D. N. Barreto, R. S. Lamarca, P. C. F. L. Gomes, J. F. da S Petruci and A. D. Batista, Novel approaches for colorimetric measurements in analytical chemistry-a review, *Anal. Chim. Acta*, 2020, **1135**, 187–203.

31 X. Lu, X. Dong, K. Zhang, X. Han, X. Fang and Y. Zhang, A gold nanorods-based fluorescent biosensor for the detection of hepatitis B virus DNA based on fluorescence resonance energy transfer, *Analyst*, 2013, **138**, 642–650.

32 K. Caswell, C. M. Bender and C. J. Murphy, Seedless, surfactantless wet chemical synthesis of silver nanowires, *Nano Lett.*, 2003, **3**, 667–669.

33 K. L. Kelly, E. Coronado, L. L. Zhao and G. C. Schatz, The optical properties of metal nanoparticles: the influence of size, shape, and dielectric environment, *J. Phys. Chem. B*, 2003, 668–677.

34 E. Oliveira, C. Núñez, H. M. Santos, J. Fernández-Lodeiro, A. Fernández-Lodeiro, J. L. Capelo and C. Lodeiro, Revisiting the use of gold and silver functionalised nanoparticles as colorimetric and fluorometric chemosensors for metal ions, *Sens. Actuators, B*, 2015, **212**, 297–328.

35 Y. Luo, X. Liu, H. Gao, Y. Li, J. Xu, F. Shen and C. Sun, Visual screening and colorimetric determination of clenbuterol and ractopamine using unmodified gold nanoparticles as probe, *J. Nanosci. Nanotechnol.*, 2016, **16**, 548–554.

36 Z. Zhou, X. Hu, X. Hong, J. Zheng, X. Liu, D. Gong and G. Zhang, Interaction characterization of 5-hydroxymethyl-2-furaldehyde with human serum albumin: binding characteristics, conformational change and mechanism, *J. Mol. Liq.*, 2020, **297**, 111835.

37 C. Liu, Q. Pang, T. Wu, W. Qi, W. Fu and Y. Wang, A Rapid Visual Detection of Ascorbic Acid through Morphology

Transformation of Silver Triangular Nanoplates, *J. Anal. Test.*, 2021, **5**, 210–216.

38 T. Lou, Z. Chen, Y. Wang and L. Chen, Blue-to-red colorimetric sensing strategy for Hg^{2+} and Ag^{+} *via* redox-regulated surface chemistry of gold nanoparticles, *ACS Appl. Mater. Interfaces*, 2011, **3**, 1568–1573.

39 J. Qi, X. Hu, X. Dong, Y. Lu, H. Lu, W. Zhao and W. Wu, Towards more accurate bioimaging of drug nanocarriers: turning aggregation-caused quenching into a useful tool, *Adv. Drug Delivery Rev.*, 2019, **143**, 206–225.

40 D.-K. Lim, I.-J. Kim and J.-M. Nam, DNA-embedded Au/Ag core–shell nanoparticles, *Chem. Commun.*, 2008, 5312–5314.

41 G. S. Métraux and C. A. Mirkin, Rapid thermal synthesis of silver nanoprisms with chemically tailorable thickness, *Adv. Mater.*, 2005, **17**, 412–415.

42 J. E. Millstone, S. J. Hurst, G. S. Métraux, J. I. Cutler and C. A. Mirkin, Colloidal gold and silver triangular nanoprisms, *Small*, 2009, **5**, 646–664.

43 X. Jiang and A. Yu, Silver nanoplates: a highly sensitive material toward inorganic anions, *Langmuir*, 2008, **24**, 4300–4309.

44 N. Cathcart, A. J. Frank and V. Kitaev, Silver nanoparticles with planar twinned defects: effect of halides for precise tuning of plasmon resonance maxima from 400 to> 900 nm, *Chem. Commun.*, 2009, 7170–7172.

45 Q. Zhang, N. Li, J. Goebl, Z. Lu and Y. Yin, A systematic study of the synthesis of silver nanoplates: is citrate a "magic" reagent?, *J. Am. Chem. Soc.*, 2011, **133**, 18931–18939.

46 A. Saadati, F. Farshchi, M. Hasanzadeh, Y. Liu and F. Seidi, Colorimetric and naked-eye detection of arsenic (III) using a paper-based colorimetric device decorated with silver nanoparticles, *RSC Adv.*, 2022, **12**, 21836–21850.

47 G. Brambilla, T. Cenci, F. Franconi, R. Galarini, A. Macrı, F. Rondoni, M. Strozzi and A. Loizzo, Clinical and pharmacological profile in a clenbuterol epidemic poisoning of contaminated beef meat in Italy, *Toxicol. Lett.*, 2000, **114**, 47–53.

48 L. Y. Yeo, H. C. Chang, P. P. Chan and J. R. Friend, Microfluidic devices for bioapplications, *Small*, 2011, **7**, 12–48.

49 G. Luka, A. Ahmadi, H. Najjaran, E. Alocilja, M. DeRosa, K. Wolthers, A. Malki, H. Aziz, A. Althani and M. Hoorfar, Microfluidics integrated biosensors: a leading technology towards lab-on-a-chip and sensing applications, *Sensors*, 2015, **15**, 30011–30031.

50 P. de Tarso Garcia, T. M. G. Cardoso, C. D. Garcia, E. Carrilho and W. K. T. Coltro, A handheld stamping process to fabricate microfluidic paper-based analytical devices with chemically modified surface for clinical assays, *RSC Adv.*, 2014, **4**, 37637–37644.

51 H. N. Baghban, M. Hasanzadeh, Y. Liu and F. Seidi, A portable colorimetric chemosensing regime for ractopamine in chicken samples using μPCD decorated by silver nanoprisms, *RSC Adv.*, 2022, **12**, 25675–25686.

52 T. A. Popov, Human exhaled breath analysis, *Ann. Allergy, Asthma, Immunol.*, 2011, **106**, 451–456.

53 S. Kazeminasab, B. Emamalizadeh, M. Khoubnasabjafari and A. Jouyban, Exhaled breath condensate: a non-invasive source for tracking of genetic and epigenetic alterations in lung diseases, *Pharmaceutical Sciences*, 2020, **27**, 149–161.

54 X. Luo, S. Zhang, Z. Xia, R. Tan, Q. Li, L. Qiao, Y. He, G. Zhang and Z. Xu, A combined surface-enhanced Raman spectroscopy (SERS)/colorimetric approach for the sensitive detection of malondialdehyde in biological samples, *Anal. Chim. Acta*, 2023, 340803.

55 J. Chen, L. Zeng, T. Xia, S. Li, T. Yan, S. Wu, G. Qiu and Z. Liu, Toward a biomarker of oxidative stress: a fluorescent probe for exogenous and endogenous malondialdehyde in living cells, *Anal. Chem.*, 2015, **87**, 8052–8056.

56 L. He, X. Yang, K. Xu and W. Lin, A mitochondria-targeted fluorescent probe for imaging endogenous malondialdehyde in HeLa cells and onion tissues, *Chem. Commun.*, 2017, **53**, 4080–4083.

57 M. Hasanzadeh, F. Mokhtari, V. Jouyban-Gharamaleki, A. Mokhtarzadeh and N. Shadjou, Electrochemical monitoring of malondialdehyde biomarker in biological samples *via* electropolymerized amino acid/chitosan nanocomposite, *J. Mol. Recognit.*, 2018, **31**, e2717.

58 C. Grazioli, G. Faura, N. Dossi, R. Toniolo, F. Tubaro, F. Terzi and G. Bontempelli, A colorimetric paper-based smart label soaked with a deep-eutectic solvent for the detection of malondialdehyde, *Sens. Actuators, B*, 2021, **329**, 129174.

59 Z. Wu, Y. Wang, Y. Wang, K. Zhang and Y. Lai, Robust and reliable detection of malondialdehyde in biological samples *via* microprobe-triggered surface-enhanced Raman spectroscopy, *Microchem. J.*, 2022, **181**, 107815.

60 X. Wang, X. Liu, T. Cheng, H. Li and X.-F. Yang, Development of 4-hydrazinyl-7-nitrobenzofurazan as a fluorogenic probe for detecting malondialdehyde in biological samples, *Sens. Actuators, B*, 2018, **254**, 248–254.

61 P. Montoro-Leal, M. Zougagh, A. Sanchez-Ruiz, A. Rios and E. V. Alonso, Magnetic graphene molecularly imprinted polypyrrole polymer (MGO@MIPy) for electrochemical sensing of malondialdehyde in serum samples, *Microchem. J.*, 2022, **178**, 107377.